

Superconductivity emerging from an electronic phase separation in the charge ordered phase of RbFe_2As_2

E. Civardi,¹ M. Moroni,¹ M. Babij,² Z. Bukowski,² and P. Carretta¹

¹*Department of Physics, University of Pavia-CNISM, I-27100 Pavia, Italy*

²*Institute of Low Temperature and Structure Research,
Polish Academy of Sciences, 50-422 Wrocław, Poland*

⁷⁵As, ⁸⁷Rb and ⁸⁵Rb nuclear quadrupole resonance (NQR) and ⁸⁷Rb nuclear magnetic resonance (NMR) measurements in RbFe_2As_2 iron-based superconductor are presented. We observe a marked broadening of ⁷⁵As NQR spectrum below $T_0 \simeq 140$ K which is associated with the onset of a charge order in the FeAs planes. Below T_0 we observe a power-law decrease in ⁷⁵As nuclear spin-lattice relaxation rate down to $T^* \simeq 20$ K. Below T^* the nuclei start to probe different dynamics owing to the different local electronic configurations induced by the charge order. A fraction of the nuclei probes spin dynamics associated with electrons approaching a localization while another fraction probes activated dynamics possibly associated with a pseudogap. These different trends are discussed in the light of an orbital selective behaviour expected for the electronic correlations.

PACS numbers: 74.70.Xa, 76.60.-k, 71.27.+a, 74.20.Mn

The parent compounds of high temperature superconducting cuprates are emblematic examples of Mott-Hubbard insulators at half band filling,[1] where the large electron Coulomb repulsion U overcomes the hopping integral t and induces both charge localization and an antiferromagnetic (AF) coupling among the spins. Electronic correlations remain sizeable even when the cuprates become superconducting and give rise to a rich phase diagram at low hole doping levels characterized by the onset of a charge density wave (CDW) which progressively fades away as the doping increases [2–5] and eventually, in the overdoped regime, a Fermi liquid scenario is restored. The comprehension of the role of electronic correlations in iron-based superconductors (IBS)[6] is more subtle. At variance with the cuprates IBS are characterized by similar nearest neighbour and next-nearest neighbour hopping integrals, the parent compounds of the most studied families of IBS (e.g. BaFe_2As_2 and LaFeAsO)[7] are not characterized by half-filled bands and, moreover, in IBS the Fermi level typically crosses five bands associated with the different Fe $3d$ orbitals, leading to a rich phenomenology in the normal as well as in the superconducting state.[7, 8] Moreover, even if signs have been reported [9, 10], the evidence for a charge order in the phase diagram of IBS still remains elusive.

Nominally, half band filling can be approached in BaFe_2As_2 IBS by replacing Ba with an alkali atom $A=\text{K}$, Rb or Cs, resulting in 5.5 electrons per Fe atom.[11] Transport measurements show that AFe_2As_2 compounds are metals[12] with sizeable electronic correlations and it has been recently pointed out that their behaviour shares many similarities with that of heavy fermion compounds.[12, 13] Indeed, the effective mass progressively increases as one moves from BaFe_2As_2 to AFe_2As_2 ,[14] even if clear discrepancies in the values derived by the different techniques are found depending on their sensitivity to the electrons from a single band or

from all the five bands.[15] de’ Medici et al. [16] pointed out that if electronic correlations are sizeable, namely U/t is of the order of the unity, the local atomic physics starts to be relevant and Hund coupling may promote the single electron occupancy of Fe d orbitals (i.e. half band-filling) and decouple the interband charge correlations. Accordingly the Mott transition becomes orbital selective[16, 17] so that while the electrons of a given band localize the electrons of other bands remain delocalized, leading to a metallic behaviour and eventually to superconductivity. This orbital selective behaviour should give rise to markedly k -dependent response functions [18] and to a sort of k -space phase separation of metallic and insulating-like domains. The point is, what happens in the real space? Will one probe the sum of the insulating and metallic response functions or should one detect a real space phase separation[19] also in AFe_2As_2 IBS [21], with different local susceptibilities? More interestingly, if electronic correlations become significant in AFe_2As_2 one could envisage the onset of a charge order[20] as in the cuprates.[2–5]

Nuclear quadrupole resonance (NQR) and nuclear magnetic resonance (NMR) are quite powerful tools which allow to probe the local response function and charge distribution. Moreover, in NQR experiments [9] the magnetic field, which often acts as a relevant perturbation, is zero. Here we show, by combining ⁷⁵As and ^{87,85}Rb NQR and ⁸⁷Rb NMR measurements, that in RbFe_2As_2 a charge order develops in the normal state below $T_0 \simeq 140$ K, possibly leading to a differentiation in real space of Fe atoms with different orbital configurations. Below T_0 , ⁷⁵As and ⁸⁷Rb nuclear spin-lattice relaxation rates ($1/T_1$) show a power law behaviour, as it is expected for a strongly correlated electron system and in good agreement with ⁷⁵As NMR results reported by Wu et al.[13]. However, at $T^* \simeq 20$ K we observe that a fraction of ⁷⁵As (or ⁸⁷Rb) nuclei probes spin dynamics char-

acteristic of a system approaching localization while others probe dynamics possibly associated with a metallic phase with a pseudogap.[23–25] Upon further decreasing the temperature the volume fraction of the heavy electron phase vanishes while the one of the metallic phase, which eventually becomes superconducting below $T_c \simeq 2.7$ K, grows. Thus, we present a neat evidence for a charge order in RbFe_2As_2 akin to underdoped cuprates. The charge order favours a phase separation into metallic and nearly insulating regions, which could result from the theoretically predicted orbital selective behaviour.[16]

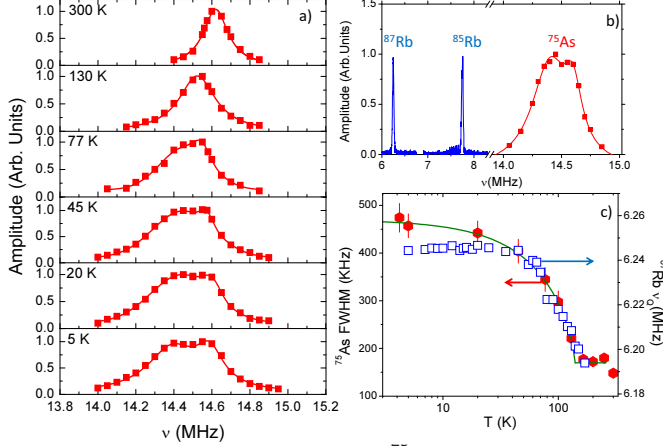


FIG. 1. (Color online) a) The ^{75}As NQR spectrum in RbFe_2As_2 is reported at different temperatures between 5 K and 300 K. The red lines are best fits with one or two (for $T < 130$ K) Lorentzians. b) The merge of the NQR spectra, associated with the $m_I = \pm 3/2 \rightarrow \pm 1/2$ transition for ^{75}As and ^{87}Rb and with the $m_I = \pm 5/2 \rightarrow \pm 3/2$ transition for ^{85}Rb ($I = 5/2$), is shown for $T = 4.2$ K. The intensity of the three spectra has been rescaled so that all three spectra have similar intensities. c) The temperature dependence of the full width at half intensity (FWHM) of ^{75}As NQR spectra (red octagons, left scale, for the plot with linear T scale see the Supplemental Material [28]) is shown together with the temperature dependence of ^{87}Rb ν_Q (blue squares, right scale). The green solid line tracking the order parameter is a phenomenological fit of the FWHM ($\Delta\nu_Q$) with $\Delta\nu_Q = 300(1 - (T/T_0))^\beta + 170$ KHz, with $T_0 = 140$ K and $\beta \simeq 0.7$.

NQR and NMR measurements were performed on a RbFe_2As_2 polycrystalline sample with a mass of about 400 mg, sealed in a quartz tube under a 0.2 bar Ar atmosphere in order to prevent deterioration. The superconducting transition temperature derived from ac susceptibility measurements turned out $T_c \simeq 2.7$ K, in good agreement with previous findings [1, 27]. Further details on the sample preparation and characterization are given in the supplemental material.[28]

First of all we shall discuss the appearance of a charge order in the FeAs planes of RbFe_2As_2 , as detected by ^{75}As NQR spectra. For a nuclear spin $I = 3/2$, as it is the case of ^{75}As and ^{87}Rb , the NQR spectrum is charac-

terized by a single line at a frequency[9]

$$\nu_Q = \frac{eQV_{ZZ}}{2h} \left(1 + \frac{\eta^2}{3}\right)^{1/2}, \quad (1)$$

with Q the nuclear quadrupole moment, V_{ZZ} the main component of the electric field gradient (EFG) tensor and η its asymmetry $\eta = (V_{XX} - V_{YY})/V_{ZZ}$. Hence the NQR spectrum probes the EFG at the nuclei generated by the surrounding charge distribution. Above 140 K, ^{75}As NQR spectrum (Fig.1) is centered around 14.6 MHz, with a linewidth of about 170 KHz, while ^{87}Rb NQR spectrum is centered around 6.2 MHz with a width of about 20 KHz. The relatively narrow NQR spectra confirms the good quality of our sample. We performed density functional theory (DFT) calculations using Elk code in the generalized gradient approximation[28] in order to derive *ab initio* the electric field gradient and NQR frequency. For ^{75}As and ^{87}Rb we obtained $(^{75}\nu_Q)_{\text{DFT}} = 14.12$ MHz and $(^{87}\nu_Q)_{\text{DFT}} = 6.7$ MHz, respectively, in reasonable agreement with the experimental values in spite of the significant electronic correlations.[37] This shows that DFT is still able to provide a fair description of the system as far as it remains a normal metal.

Upon cooling the sample below $T_0 \simeq 140$ K significant changes are detected in ^{75}As NQR spectra (Fig. 1). The spectrum is observed to progressively broaden with decreasing temperature and below 50 K one clearly observes that the spectrum is actually formed by two humps nearly symmetrically shifted with respect to the center (Fig.1a). The presence of two peaks in the ^{75}As NQR spectra has already been detected in different families of IBS and associated with a nanoscopic phase separation in regions characterized by different electron doping levels.[38] However, at variance with what we observe here, the two peaks observed in other IBS do not show the same intensity [38] and the spectra show little temperature dependence, namely the nanoscopic phase separation is likely pinned. Under both high magnetic field and high pressure an asymmetric splitting of ^{75}As NMR spectrum was detected also in KFe_2As_2 which, however, is absent in zero field (NQR).[10] Here we observe the emergence of an NQR spectrum which recalls the one expected for an incommensurate CDW,[39–41] which causes a periodic modulation of the EFG at the nuclei and gives rise to two symmetrically shifted peaks in the spectrum. The EFG modulation could involve also the onset of an orbital order[42] or a structural distortion, possibly coupled to the charge order. Although it is not straightforward from our data to discriminate among these scenarios, it is clear that we detect a symmetry breaking below T_0 to a low temperature phase characterized by a spatial modulation of the EFG, namely by a charge order.

^{87}Rb NQR spectrum does not show a significant broadening upon decreasing the temperature but is characterized by a ν_Q which, at $T > T^* \simeq 20 - 25$ K, shows a temperature dependence similar to that of the ^{75}As NQR

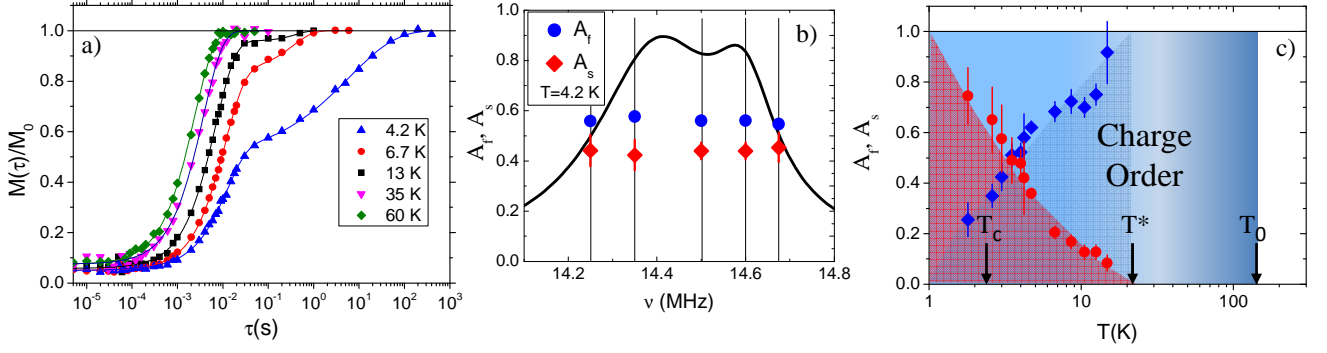


FIG. 2. (Color online) a) The recovery of ^{75}As nuclear magnetization $M(\tau)$ (measured in NQR) is reported as a function of the delay τ between a saturation radiofrequency pulse sequence and the echo readout sequence for different temperatures. The solid lines are the best fits according to Eq.2 in the text. b) The frequency dependence of the fraction of fast A_f and slow relaxing A_s nuclei is reported as a function of the irradiation frequency across ^{75}As NQR spectrum. The black solid lines is the best fit of the spectrum at $T = 4.2$ K. c) The temperature dependence of A_f (blue) and A_s (red) recorded on the low-frequency peak of the ^{75}As NQR spectrum.

spectra full width at half maximum (FWHM), proportional to the charge order parameter (Fig.1c). Below T^* ^{87}Rb ν_Q flattens and deviates from ^{75}As NQR FWHM. The fact that the NQR spectrum of the out of plane ^{87}Rb nuclei is less sensitive than ^{75}As one to the charge order is an indication that the order develops in the FeAs planes and that the modulation of the EFG at ^{75}As nuclei should occur over a few lattice steps, otherwise one should expect a splitting also of the narrow ^{87}Rb NQR spectrum. It is interesting to notice that at a temperature of the order of T^* an abrupt change in the uniaxial thermal expansion occurs,[43] evidencing also a change in the lattice properties.

Now we discuss the temperature dependence of the low-energy dynamics probed by ^{75}As and ^{87}Rb $1/T_1$. The nuclear spin-lattice relaxation rate was determined from the recovery of the nuclear magnetization after exciting the nuclear spins with a saturation recovery pulse sequence. The recovery of ^{75}As magnetization in NQR is shown in Fig.2a. One notices that a single exponential recovery describes very well the recovery of the nuclear magnetization at $T \geq 20$ K, as it can be expected for a homogeneous system where all nuclei probe the same dynamics. However, below $T^* \simeq 20$ K one observes the appearance of a second component characterized by much longer relaxation times. Namely, a part of the nuclei probes dynamics causing a fast relaxation ($1/T_1^f$) and a part of the nuclei a slow relaxation ($1/T_1^s$). Accordingly, the recovery was fit to

$$M(\tau) = M_0 \left[1 - f \left(A_f e^{-3\tau/T_1^f} + A_s e^{(-3\tau/T_1^s)^\beta} \right) \right], \quad (2)$$

with M_0 the nuclear magnetization at thermal equilibrium, A_f and A_s the fraction of fast relaxing and slow relaxing nuclei, respectively, f a factor accounting for a non perfect saturation by the radiofrequency pulses and $0.8 \geq \beta \geq 0.3$ a stretching exponent characterizing the

slowly relaxing component. As the temperature is lowered one observes a progressive increase of A_s with respect to A_f and at the lowest temperature ($T = 1.7$ K), about 80% of the nuclei are characterized by the slow relaxation (Fig.2c). It is important to notice that in RbFe_2As_2 Wu et al.[13] (in NMR, not in NQR) did not observe a clear separation of the recovery in two components as we do here but they did observe deviations from a single exponential recovery below 20 K which, however, were fitted with a stretched exponential, likely yielding an average $1/T_1$ value between $1/T_1^s$ and $1/T_1^f$. Remarkably also ^{87}Rb NMR $1/T_1$ clearly shows two components below 25 K and just one above.[28]

^{75}As $1/T_1$ was measured both on the high frequency and on the low-frequency shoulder of the NQR spectrum and it was found to be the same (Fig.3a) over a broad temperature range. Moreover, at $T = 4.2$ K we carefully checked the frequency dependence of T_1^f , T_1^s , A_f and A_s and found that neither the two relaxation rates nor their amplitude vary across the spectrum (Fig.2b, see also Ref.28). This means that nuclei resonating at different frequencies probe the same dynamics which implies that the charge modulation induced by the charge order has a nanoscopic periodicity.[38] One could argue that the two components are actually present at all temperatures but that they arise only at low temperature once nuclear spin diffusion[44] is no longer able to establish a common spin temperature (i.e. a common T_1) among the nuclei resonating at different frequencies. However, we remark that since the nuclear spin-spin relaxation rate ($1/T_2$) is constant [28] and the width of the NQR spectrum is nearly constant below 40 K (Fig.1c) the poor efficiency of nuclear spin diffusion should not vary, at least for $T \leq 40$ K. Hence, the appearance of different relaxation rates below T^* should arise from a phase separation causing a slight change in the average electronic charge distribution causing little effect on the NQR spectra (see Fig. 1) but a

marked differentiation in the low-energy excitations [18], which starts to be significant at low temperature once the effect of electronic correlations is relevant.

One has to clarify if the relaxation mechanism is magnetic, driven by electron spin fluctuations, or quadrupolar, driven by EFG fluctuations, typically induced by CDW amplitude and phase modes.[41] In order to clarify this point we measured the ratio between ^{87}Rb and ^{85}Rb $1/T_1$ (fast component) at a few selected temperatures below 25 K. The ratio $^{87}(1/T_1)/^{85}(1/T_1) = 12 \pm 1$, in good agreement with the ratio between the square of the gyromagnetic ratios of the two nuclei $(^{87}\gamma/^{85}\gamma)^2 = 11.485$, showing that the relaxation is driven by the correlated spin fluctuations and not by charge fluctuations associated with CDW excitations. Since ^{75}As shows a temperature dependence of the relaxation analogous to the one of ^{87}Rb (Fig.3a) we argue that also ^{75}As $1/T_1$ is driven by spin fluctuations. Thus we can write that

$$\frac{1}{T_1} = \frac{\gamma_n^2}{2\hbar} k_B T \frac{1}{N} \sum_{\vec{q}} |A_{\vec{q}}|^2 \frac{\chi''(\vec{q}, \omega_0)}{\omega_0}, \quad (3)$$

with $|A_{\vec{q}}|^2$ the form factor giving the hyperfine coupling with the collective spin excitations at wave-vector \vec{q} , and $\chi''(\vec{q}, \omega_0)$ the imaginary part of the dynamic susceptibility at the resonance frequency ω_0 .

Now we turn to the temperature dependence of $1/T_1$ above $T^* \simeq 20$ K and of $1/T_1^s$ and $1/T_1^f$ below that temperature. Above T^* $1/T_1$ increases with a power law $1/T_1 = aT^b$, with $b = 0.79 \pm 0.01$ for ^{75}As , and flattens around $T_0 \simeq 140$ K (Fig.3a), in very good agreement with the results reported by Wu et al.[13] from ^{75}As NMR. Notice that T_0 corresponds to the temperature below which we start to observe a significant broadening of ^{75}As NQR spectrum. Hence, the power law behaviour of $1/T_1$ seems to arise from the onset of the charge order.

Below $T^* \simeq 20$ K $1/T_1^f$ deviates from the power law behaviour and progressively flattens on decreasing temperature (Fig.3a). The same behaviour is detected for ^{87}Rb NMR $1/T_1$, although the flattening starts at a higher temperature, suggesting that T^* might be field dependent. On the other hand, $1/T_1^s$ gets progressively longer as the temperature is lowered and follows an activated trend with an energy barrier $E_g = 17 \pm 0.9$ K.

The behaviour of $1/T_1^f$ is characteristic of a system approaching a QCP where localization occurs. In fact, from Moriya self-consistent renormalization (SCR) approach for a quasi-2D system with AF correlations, one should have $1/T_1 = T\chi(Q)$, [45, 46] with $\chi(Q)$ the static susceptibility at the AF wave-vector. In the proximity of the QCP $\chi(Q) \sim \ln(1/T)/T$, leading to a weak logarithmic divergence of $1/T_1 \sim \ln(1/T)$ for $T \rightarrow 0$, while at higher temperature $\chi(Q)$ should show a Curie-Weiss behaviour, yielding a nearly flat $1/T_1$, as we do observe in RbFe_2As_2 (Fig.3a). The corresponding behaviour of $1/T_1^f T$ is reported in Fig.3b.

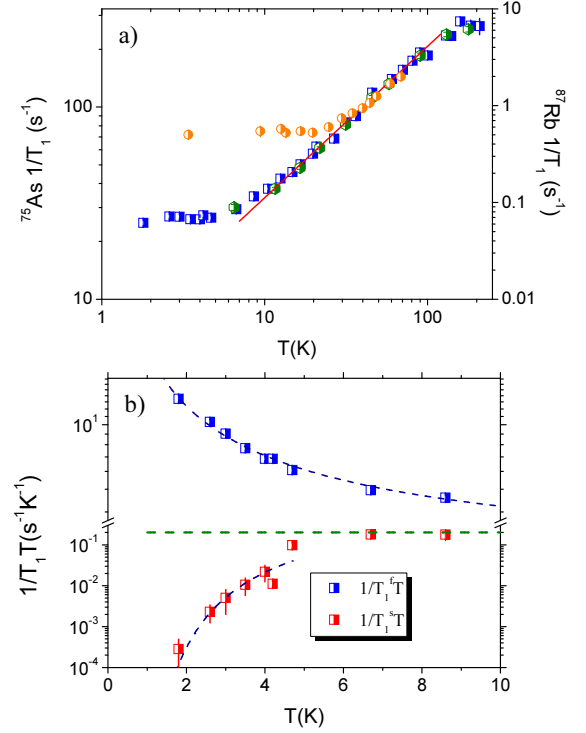


FIG. 3. (Color online) a) The temperature dependence of ^{75}As NQR $1/T_1$ in RbFe_2As_2 , for $T \geq 20$ K, and of the fast relaxation rate $1/T_1^f$, for $T < 20$ K, are reported for an irradiation frequency centered at the low-frequency peak (blue squares) and for an irradiation frequency centered at the high frequency peak (green circles). The red solid line is a best fit to the data between 20 and 100 K with a power law characterized by an exponent $b = 0.79$. ^{87}Rb NMR $1/T_1$ (orange circles) in RbFe_2As_2 is reported between 3.5 and 70 K, for an external magnetic field $H = 7$ Tesla. b) The temperature dependence of ^{75}As NQR $1/T_1^f T$ (blue squares) and $1/T_1^s T$ (red circles) in RbFe_2As_2 is reported. The dashed line at the bottom is the best fit according to an activated behaviour with an energy gap $E_g = 17 \pm 0.9$ K. The dashed line at the top is the behaviour expected according to Moriya SCR theory (see text). The dashed horizontal line shows schematically the Korringa-like behaviour expected for an uncorrelated metal.

On the other hand, $1/T_1^s T$, corresponding to the relaxation rate of the majority phase at low temperature, shows the opposite trend (Fig.3b), decreasing upon cooling. Being the system metallic at low temperature, the deviation of $1/T_1^s T$ from the constant Korringa-like behaviour [9] expected for a metal should possibly be associated with the opening of a pseudogap, similarly to what one observes in the underdoped regime of the cuprates,[23–25] and in agreement with theoretical predictions for hole-doped IBS.[18]

In conclusion, our results show that, akin to cuprates, a charge order develops also in the normal state of IBS when the electronic correlations are sizeable. Accordingly, the presence of a charge order appears to be a common feature in the phase diagram of cuprate and iron-based superconductors and could play a key role in

determining the superconducting state properties.[20, 47] Moreover, we observe a local electronic separation in two phases characterized by different excitations which could possibly be explained in terms of the orbital selective behaviour[16] predicted for IBS. Finally we remark that the occurrence of an electronic phase separation is theoretically supported by a recent study of the electron fluid compressibility. [48]

ACKNOWLEDGMENTS

Massimo Capone is thanked for useful discussions. The Sezione INFN di Pavia is acknowledged for granting the computing time necessary to perform DFT calculations. This work was supported by MIUR-PRIN2012 Project No. 2012X3YFZ2.

-
- [1] N. F. Mott, Proc. Phys. Soc. London, Sect. A **62**, 416 (1949).
 - [2] T. Wu, H. Mayaffre, S. Krämer, M. Horvatić, C. Berthier, W.N. Hardy, R. Liang, D.A. Bonn, and M.-H. Julien, Nature (London) **477**, 191 (2011).
 - [3] J.M. Tranquada, B.J. Sternlieb, J.D. Axe, Y. Nakamura and S. Uchida, Nature **375**, 561 (1995).
 - [4] G. Ghiringhelli, M. Le Tacon, M. Minola, S. Blanco-Canosa, C. Mazzoli, N.B. Brookes, G.M. De Luca, A. Frano, D.G. Hawthorn, F. He, T. Loew, M. Moretti Sala, D.C. Peets, M. Salluzzo, E. Schierle, R. Sutarto, G.A. Sawatzky, E. Weschke, B. Keimer and L. Braicovich, Science **337**, 821 (2012).
 - [5] M. Hücker, N.B. Christensen, A.T. Holmes, E. Blackburn, E.M. Forgan, R. Liang, D.A. Bonn, W.N. Hardy, O. Gutowski, M. v. Zimmermann, S.M. Hayden and J. Chang, Phys. Rev. B **90**, 054514 (2014).
 - [6] Y. Kamihara, T. Watanabe, M. Hirano, and H. Hosono, J. Am. Chem. Soc. **130**, 3296 (2008).
 - [7] D.C. Johnston, Adv. Phys. **59**, 803 (2010).
 - [8] I. I. Mazin, D. J. Singh, M. D. Johannes, and M. H. Du, Phys. Rev. Lett. **101**, 057003 (2008); K. Kuroki, S. Onari, R. Arita, H. Usui, Y. Tanaka, H. Kontani, and H. Aoki, Phys.Rev.Lett. **101**, 087004 (2008).
 - [9] A.K. Jasek, K. Komadera, A. Blachowski, K. Ruebenbauer, Z. Bukowski, J.G. Storey and J. Karpinski, J. Alloys Comp. **609**, 150 (2014)
 - [10] P. S. Wang, P. Zhou, J. Dai, J. Zhang, X. X. Ding, H. Lin, H. H. Wen, B. Normand, R. Yu, and W. Yu, Phys. Rev. B **93**, 085129 (2016).
 - [11] F. F. Tafti, A. Ouellet, A. Juneau-Fecteau, S. Faucher, M. Lapointe-Major, N. Doiron-Leyraud, A. F. Wang, X.-G. Luo, X. H. Chen, and L. Taillefer, Phys. Rev. B **91**, 054511 (2015).
 - [12] F. Eilers, K. Grube, D. A. Zocco, T. Wolf, M. Merz, P. Schweiss, R. Heid, R. Eder, R. Yu, J.-X. Zhu, Q. Si, T. Shibauchi, and H. v. Löhneysen, Phys. Rev. Lett. **116**, 237003 (2016)
 - [13] Y. P. Wu, D. Zhao, A. F. Wang, N. Z. Wang, Z. J. Xiang, X. G. Luo, T. Wu, and X. H. Chen, Phys.Rev.Lett. **116**, 147001 (2016); see also the corresponding Supplemental Material at <http://journals.aps.org/prl/supplemental/10.1103/PhysRevLett.116.147001>
 - [14] A. K. Pramanik, M. Abdel-Hafez, S. Aswartham, A. U. B. Wolter, S. Wurmehl, V. Kataev, and B. Büchner, Phys. Rev. B **84**, 064525 (2011).
 - [15] G. Li, W. Z. Hu, J. Dong, Z. Li, P. Zheng, G. F. Chen, J. L. Luo, and N. L. Wang, Phys. Rev. Lett. **101**, 107004 (2008); M. Yi, D. H. Lu, J. G. Analytis, J.-H. Chu, S.-K. Mo, R.-H. He, R. G. Moore, X. J. Zhou, G. F. Chen, J. L. Luo, N. L. Wang, Z. Hussain, D. J. Singh, I. R. Fisher, and Z.-X. Shen, Phys. Rev. B **80**, 024515 (2009).
 - [16] L. de' Medici, S.R. Hassan, M. Capone and X. Dai, Phys.Rev.Lett. **102**, 126401 (2009)
 - [17] L. de' Medici, G. Giovannetti and M. Capone, Phys.Rev.Lett. **112**, 177001 (2014)
 - [18] E. Gull, M. Ferrero, O. Parcollet, A. Georges, and A. J. Millis, Phys. Rev. B **82**, 155101 (2010).
 - [19] V. J. Emery and S.A. Kivelson, Physica C **209**, 597 (1993); U. Low, V. J. Emery, K. Fabricius, and S.A. Kivelson, Phys. Rev. Lett. **72**, 1918 (1994).
 - [20] C. Castellani, C. Di Castro and M. Grilli, Phys. Rev. Lett. **75**, 4650 (1995).
 - [21] E. Dagotto, A. Moreo, A. Nicholson, Q. Luo, S. Liang and X. Zhang, Front. Phys. **6**, 379 (2011)
 - [22] A. Abragam, in *Principles of Nuclear Magnetism*, Oxford University Press (1983).
 - [23] H. Alloul, T. Ohno and P. Mendels, Phys. Rev. Lett. **63**, 1700 (1989).
 - [24] H. Ding, T. Yokoya, J.C. Campuzano, T. Takahashi, M. Randeira, M.R. Norman, T. Mochiku, H. Kadowaki and J. Giapintzakis, Nature **382**, 51 (1996).
 - [25] B. Batlogg, H. Y. Hwang, H. Takagi, R.J. Cava, H.L. Kao and J. Kwo, Physica C **235-240**, 130 (1994).
 - [26] Z. Bukowski, S. Weyeneth, R. Puzniak, J. Karpinski and B. Batlogg, Physica C **470**, S328 (2010).
 - [27] Z. Shermadini, H. Luetkens, A. Maisuradze, R. Khasanov, Z. Bukowski, H.-H. Klauss, and A. Amato, Phys. Rev. B **86**, 174516 (2012).
 - [28] For details on the sample preparation and characterization, DFT calculations as well as on NQR and NMR measurements see the Supplemental Material [url] which includes Refs. [29-36].
 - [29] Elk code, version 3.3.17, <http://elk.sourceforge.net>
 - [30] J. P. Perdew, A. Ruzsinszky, G. I. Csonka, O. A. Vydrov, G. E. Scuseria, L. A. Constantin, X. Zhou, and K. Burke, Phys. Rev. Lett. **100**, 136406 (2008)
 - [31] H. J. Monkhorst and J. D. Pack, Phys. Rev. B **13**, 5188 (1976).
 - [32] M. Methfessel and A. Paxton, Phys. Rev. B **40**, 3616 (1989).
 - [33] J.A. Lehmann-Horn, R. Yong, D.G. Miljak and T.J. Bastow, Solid State Nucl. Mag. Res. **71**, 87 (2015)
 - [34] R. E. Walstedt and S.-W. Cheong, Phys. Rev. B **51**, 3163 (1995).
 - [35] L. Bossoni, P. Carretta, W. P. Halperin, S. Oh, A. Reyes, P. Kuhns, and P. C. Canfield, Phys. Rev. B **88**, 100503 (2013).
 - [36] D.E. MacLaughlin, J.D. Williamson and J. Butterworth, Phys. Rev. B **4**, 60 (1971).
 - [37] S. Backes, H.O. Jeschke, and R. Valenti, Phys. Rev. B **92**, 195128 (2015).

- [38] G. Lang, H.-J. Grafe, D. Paar, F. Hammerath, K. Manthey, G. Behr, J. Werner, and B. Büchner, Phys. Rev. Lett. **104**, 097001 (2010).
- [39] P. Butaud, P. Ségransan, C. Berthier, J. Dumas, and C. Schlenker, Phys. Rev. Lett. **55**, 253 (1985).
- [40] J. H. Ross, Z. Wang, and C.P. Slichter Phys. Rev. Lett. **56**, 663 (1986)
- [41] C. Berthier and P. Ségransan, in *Low-dimensional Conductors and Superconductors*, Eds. D.Jérôme and L.G.Caron, (Plenum Pub., 1987), p.455
- [42] K.I. Kugel and D.I. Khomskii, Sov. Phys.-JETP **37**, 725 (1973)
- [43] F. Hardy, A.E. Böhrer, L. de' Medici, M. Capone, G. Giovannetti, R. Eder, L. Wang, M. He, T. Wolf, P. Schweiss, R. Heid, A. Herbig, P. Adelmann, R. A. Fisher, and C. Meingast, arXiv:1605.05485
- [44] W.E. Blumberg, Phys. Rev. **119**, 79 (1960)
- [45] A. Ishigaki and T. T. Moriya, J. Phys. Soc. Jpn. **65**, 3402 (1996); ibid. **67**, 3924 (1998).
- [46] F. Hammerath, P. Bonfá, S. Sanna, G. Prando, R. De Renzi, Y. Kobayashi, M. Sato, and P. Carretta, Phys. Rev. B **89**, 134503 (2014).
- [47] S. Caprara, C. Di Castro, G. Seibold and M. Grilli, arXiv:1604.07852v1
- [48] L. de' Medici, arXiv:1609.01303v1

SUPPLEMENTARY MATERIAL

I. SAMPLE SYNTHESIS AND CHARACTERIZATION

A polycrystalline sample of RbFe_2As_2 was synthesized in two steps.[1] First, RbAs and Fe_2As precursors were prepared from stoichiometric amounts of rubidium, arsenic and iron. The components were mixed and heated in evacuated and sealed silica tubes at 350 C and at 800 C, respectively. Then, the obtained RbAs and Fe_2As were mixed together in a molar ratio 1:1, pressed into pellets and placed in an alumina crucible and sealed in an evacuated silica ampoule. The sample was annealed at 650 C for three days, ground and annealed for another three days at the same temperature. It should be emphasized that the annealing temperature and time are crucial parameters. The annealing at higher temperature or extended annealing time causes decomposition of the compound.

The phase purity was checked by X-ray powder diffraction. The diffraction lines (shown in Fig.4) can be indexed with a tetragonal ThCr_2Si_2 type unit cell with lattice parameters $a = 3.871 \text{ \AA}$ and $c = 14.464 \text{ \AA}$, in good agreement with those reported in Ref.1. The ac-susceptibility measurements were performed on heating with an ac field of 10 Oe at 1111 Hz. The real component (Fig.5) reveals the onset of diamagnetism and of bulk superconductivity below $T_c \simeq 2.7 \text{ K}$. [1]

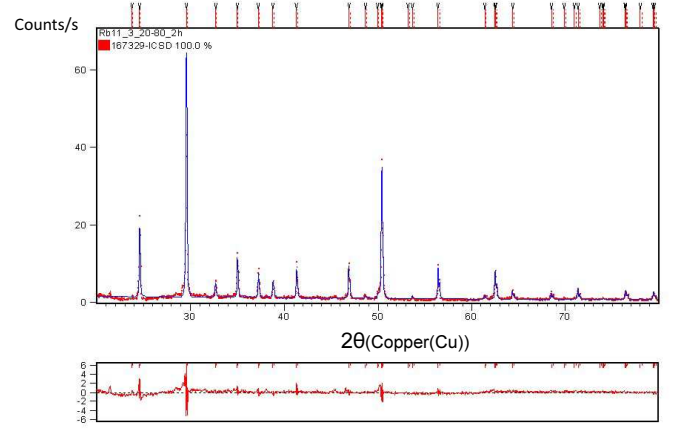


FIG. 4. RbFe_2As_2 room temperature X-ray diffraction pattern.

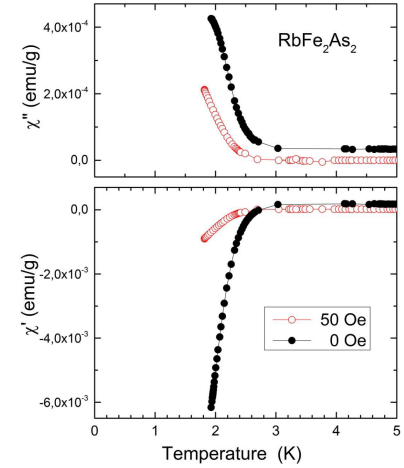


FIG. 5. Temperature dependence of the real (χ') and imaginary part (χ'') of the ac susceptibility close to T_c in RbFe_2As_2 in zero field and for a static external magnetic field of 50 Oe.

II. DFT CALCULATIONS

First-principles DFT calculations of the electronic structure were performed using the full-potential linearized augmented plane-wave method as implemented in the Elk package [2]. For the exchange-correlation functional we used the generalized gradient approximation of Perdew, Burke, and Ernzerhof [3]. The atomic positions used in the calculation are those obtained from room temperature x-ray diffraction. In order to calculate the electric field gradient (EFG) tensor components V_{ij}^α we solved the Poisson equation for the charge distribution to determine the electrostatic potential φ and derived V_{ij}^α from

$$V_{ij}^\alpha = \left. \frac{\partial^2 \varphi}{\partial \mathbf{r}_i \partial \mathbf{r}_j} \right|_{\mathbf{r}_\alpha}, \quad (4)$$

where α runs over the nuclei at \mathbf{r}_α . Since the EFG tensor is extremely sensitive to the charge distribution a well converged basis set is needed to grant the convergence with respect to the EFG tensor components. We used muffin tin radii of $2.6 a_0$ for Rb and $2.4 a_0$ for Fe and As, with $R_{min}^{MT} \times \max(|k|) = 9$, where R_{min}^{MT} is the smallest muffin tin (MT) radius inside the MT spheres and $|k|$ the magnitude of the reciprocal space vectors. We choose 9 for the cut off of the angular momentum quantum number in the lattice harmonics expansion inside the MTs. Reciprocal space was sampled with the Monkhorst-Pack [4] scheme on a $24 \times 24 \times 24$ grid. A smearing of 270 meV was used within the Methfessel-Paxton scheme [5] and convergence of the EFG components with respect to all these parameters has been carefully checked. Once the EFG tensor components are known the NQR frequency at ^{75}As and ^{87}Rb can be calculated from Eq. 1 in the main article. The obtained values, $(^{75}\nu_Q)_{\text{DFT}} = 14.12$ MHz and $(^{87}\nu_Q)_{\text{DFT}} = 6.7$ MHz are in good agreement with the experimental values $(^{75}\nu_Q)_{\text{exp}} = 14.6$ MHz and $(^{87}\nu_Q)_{\text{exp}} = 6.2$ MHz and the discrepancy represents an estimate of the accuracy of the DFT calculation which is known to not properly account for the electronic correlations.

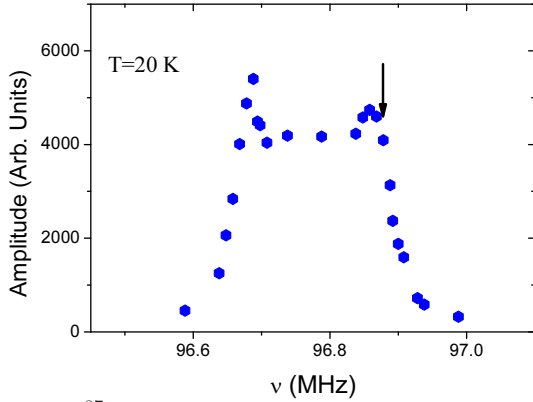


FIG. 6. ^{87}Rb NMR powder spectrum in RbFe_2As_2 for the central $m_I = 1/2 \rightarrow -1/2$ transition is shown for $T = 20$ K. The arrow marks the position where ^{87}Rb NMR $1/T_1$ was measured.

III. NQR AND NMR SPECTRA

^{75}As NQR and ^{87}Rb NMR spectra were derived by recording the integral of the echo signal after a $\pi/2 - \tau_e - \pi$ pulse sequence as a function of the irradiation frequency. At a few temperatures the ^{75}As NQR spectra was also obtained by merging the Fourier transforms of half of the echo recorded at different frequencies but no relevant additional features appeared in the spectra. We point out that any tiny amount of spurious phases as FeAs and Fe_2As (not detected in X-ray diffraction) will not affect the ^{75}As NQR spectra since these materials are magnet-

ically ordered and the internal field shifts the resonance frequency to much higher values. Also in FeAs_2 the ^{75}As NQR line is in a completely different frequency range.[6]

The narrow $^{87,85}\text{Rb}$ NQR spectra were obtained from the Fourier transform of half of the echo signal obtained after the same echo pulse sequence. ^{87}Rb NMR powder spectrum for the central $m_I = 1/2 \rightarrow -1/2$ transition is displayed in Fig.6. The spectrum is fully compatible with the ^{87}Rb quadrupole frequency determined from the NQR spectra.

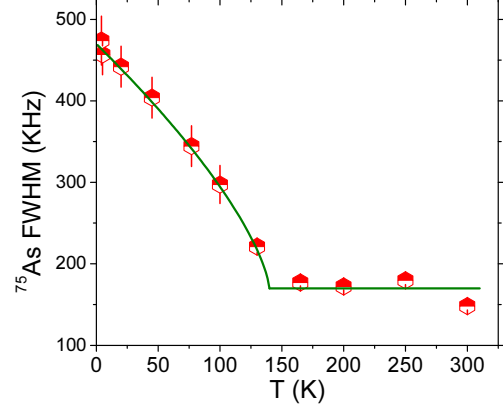


FIG. 7. The temperature dependence of ^{75}As NQR spectrum full width at half maximum (FWHM) in RbFe_2As_2 is reported. The green solid line tracking the order parameter is a phenomenological fit of ^{75}As NQR FWHM ($\Delta\nu_Q$) with $\Delta\nu_Q = 300(1 - (T/T_0))^\beta + 170$ KHz, with $T_0 = 140$ K and $\beta \simeq 0.7$.

IV. SPIN-SPIN RELAXATION RATE $1/T_2$

^{75}As spin-spin relaxation rate $1/T_2$ was derived in NQR by recording the decay of the echo amplitude $E(2\tau_e)$ after a $\pi/2 - \tau_e - \pi$ pulse sequence. The decay could be fit in general with $E(2\tau_e) = E(0)\exp(-2\tau_e/T_2^e)^\beta$ with $\beta \simeq 1.6$. A value of β lower than 2 and the slight temperature dependence of $1/T_2^e$ (Fig.8) should be associated with Redfield contribution to the relaxation $1/T_{2R}$. Then one can write $E(2\tau_e) = E(0)\exp(-2\tau_e/T_2)^\beta \exp(-2\tau_e/T_{2R})$, with $1/T_2$ the spin-spin relaxation rate. In case of an anisotropic spin-lattice relaxation rate, Walstedt *et al.* [7] calculated a general expression for $1/T_{2R}$. In case of a nuclear spin $I = 3/2$, with the Z axes of the EFG along the c axes one should have:

$$\frac{1}{T_{2R}} = \frac{3}{T_1^{\parallel c}} + \frac{1}{T_1^{\perp c}} \quad (5)$$

where the symbols \parallel and \perp refers to the external field orientation with respect to the crystallographic c axis. In particular, $1/T_1^{\parallel c}$ corresponds to ^{75}As NQR $1/T_1$. $1/T_1^{\perp c}$ was determined by assuming an anisotropy in $1/T_1$ equal to the one found in electron-doped BaFe_2As_2 [8]. Once

the data have been corrected by Redfield contribution one finds that ^{75}As $1/T_2$ is temperature independent (Fig.8), with $\beta_2 \simeq 1.8$. The deviation of β_2 from 2, as it is expected in the case of nuclear dipolar interaction in a dense system [9] is likely a consequence of the partial irradiation of the NQR spectrum.

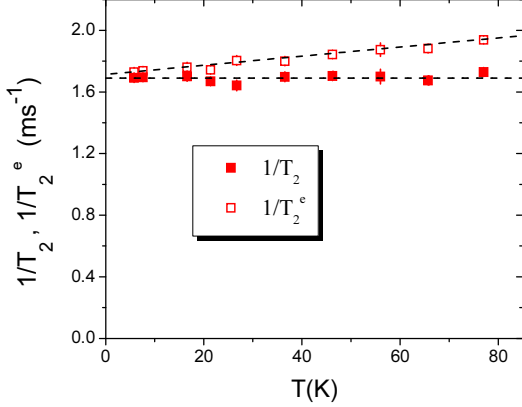


FIG. 8. The temperature dependence of ^{75}As NQR $1/T_2^e$ (open squares) and $1/T_2$ (closed squares), after Redfield correction, for RbFe_2As_2 is reported. The dashed lines are guide to the eye.

Taking into account of T_2 corrections we have measured the T -dependence of ^{75}As NQR spectrum amplitude below 50 K and did not observe any significant change.

V. NUCLEAR SPIN-LATTICE RELAXATION RATE $1/T_1$

^{87}Rb NMR $1/T_1$ was measured in a $H = 7$ Tesla magnetic field by irradiating just the high frequency shoulder of the powder spectrum of the central line shown in Fig.6, corresponding to grains with the c -axes perpendicular to \vec{H} . The recovery of ^{87}Rb NMR central line magnetization after a saturation recovery pulse sequence was fit according to

$$M(\tau) = M_0 \left(1 - f(0.9e^{-6\tau/T_1} + 0.1e^{-\tau/T_1}) \right). \quad (6)$$

The recovery is shown in Fig.9 and one observes, similarly to what one finds in ^{75}As NQR, two components appearing at low temperature.

The long component were measured just in NMR since in NQR the very long ^{87}Rb relaxations and the much lower signal intensity make the measurements quite demanding. The fast component, the only one present at $T > 25$ K, was measured in NQR irradiating either ^{87}Rb $\pm 3/2 \rightarrow \pm 1/2$ transition or ^{85}Rb $\pm 5/2 \rightarrow \pm 3/2$. The recovery of nuclear magnetization was fit according to the recovery laws expected for a magnetic relaxation mechanism [10]

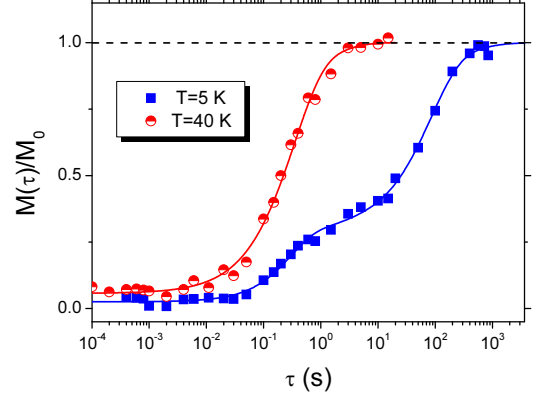


FIG. 9. The recovery of ^{87}Rb NMR magnetization after a saturation pulse sequence, when the high frequency peak of the NMR spectrum for the central $1/2 \rightarrow -1/2$ transition is irradiated, at $T = 40$ K (red circles) and at $T = 5$ K (blue squares). The solid lines are the best fits according to Eq. 6, for $T = 40$ K, and according to the same recovery law, but considering two components, for $T = 5$ K.

nism [10]

$$M(\tau) = M_0 \left(1 - f e^{-3\tau/T_1} \right), \quad (7)$$

for ^{87}Rb and

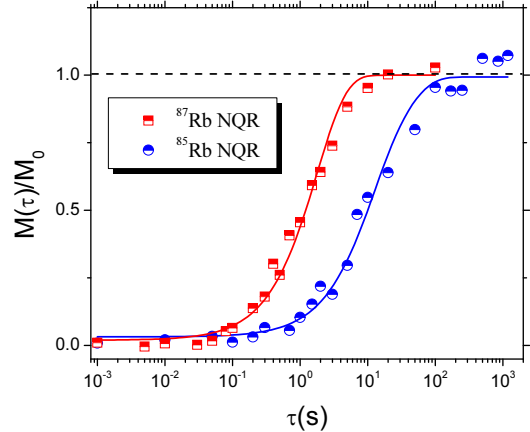


FIG. 10. The recovery of ^{87}Rb (red squares) and of ^{85}Rb (blue circles, $\pm 5/2 \rightarrow \pm 3/2$ transition) magnetization in NQR after a saturation pulse sequence, for $T = 4.2$ K. The solid lines are the best fits according to Eqs. 7 and 8, respectively. Although the recovery law (Eq.8) for ^{85}Rb would imply a faster recovery, it is clear that ^{87}Rb relaxation is much faster as it is expected for a magnetic relaxation mechanism.

$$M(\tau) = M_0 \left(1 - f(0.427e^{-3\tau/T_1} + 0.573e^{-10\tau/T_1}) \right), \quad (8)$$

for ^{85}Rb . The ratio between the $1/T_1$ of the two nuclei for the fast relaxing component was measured at a few selected temperatures between 4 and 25 K and

$^{87}(1/T_1)/^{85}(1/T_1) = 12 \pm 1$ (Fig.10), in good agreement with the ratio between the square of the gyromagnetic ratios of the two nuclei ($^{87}\gamma/^{85}\gamma)^2 = 11.485$, confirming the adequacy of the recovery laws we have used to estimate $1/T_1$ and the fact that the relaxation is driven by electron spin fluctuations. Notice that if the relaxation was driven by EFG fluctuations $1/T_1$ should scale with the square of the nuclear electric quadrupole moment and one should have $^{87}(1/T_1)/^{85}(1/T_1) = 0.226$ a value about 50 times smaller than the experimental one.

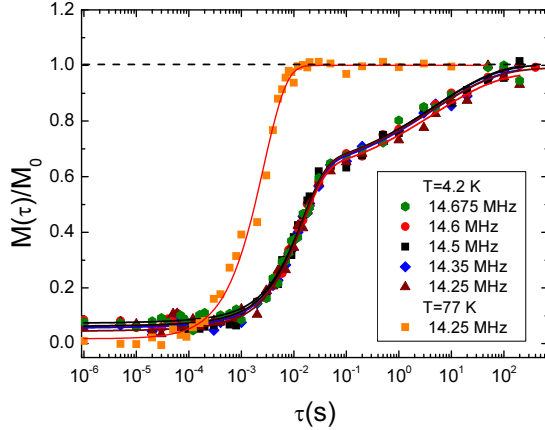


FIG. 11. The recovery of ^{75}As NQR magnetization after a saturation pulse sequence for different irradiation frequencies across the NQR spectrum, at $T = 4.2$ K. The single exponential recovery law for $T = 77$ K is reported up to times longer than $10^3 T_1$. The solid lines are best fits according to Eq.2 in the main article.

We have measured the frequency dependence of ^{75}As $1/T_1$ across the NQR spectrum by decreasing the intensity of the radiofrequency field so that we irradiated a

width of about 30 KHz in the spectrum. We found that the recovery laws did not change significantly across the spectrum (Fig.11). Namely, A_f , A_s , $1/T_1^f$ and $1/T_1^s$ show a negligible frequency dependence. It should be mentioned that A_s and A_f appear to slightly depend on the thermal history (i.e. on the cooling rate), an aspect that will be the subject of future studies. Finally, we have checked that A_s , the amplitude of the slow relaxing component, is zero above 20 K by recording the recovery up to more than $10^3 T_1$ (Fig.11).

-
- [1] Z. Bukowski, S. Weyeneth, R. Puzniak, J. Karpinski and B. Batlogg, *Physica C* **470**, S328 (2010).
 - [2] Elk code, version 3.3.17, <http://elk.sourceforge.net>
 - [3] J. P. Perdew, A. Ruzsinszky, G. I. Csonka, O. A. Vydrov, G. E. Scuseria, L. A. Constantin, X. Zhou, and K. Burke, *Phys. Rev. Lett.* **100**, 136406 (2008)
 - [4] H. J. Monkhorst and J. D. Pack, *Phys. Rev. B* **13**, 5188 (1976).
 - [5] M. Methfessel and A. Paxton, *Phys. Rev. B* **40**, 3616 (1989).
 - [6] J.A. Lehmann-Horn, R.Yong, D.G.Miljak and T.J.Bastow, *Solid State Nucl. Mag. Res.* **71**, 87 (2015)
 - [7] R. E. Walstedt and S.-W. Cheong, *Phys. Rev. B* **51**, 3163 (1995).
 - [8] L. Bossoni, P. Carretta, W. P. Halperin, S. Oh, A. Reyes, P. Kuhns, and P. C. Canfield, *Phys. Rev. B* **88**, 100503 (2013).
 - [9] A. Abragam in *Principles of Nuclear Magnetism*, (Oxford University Press 1983).
 - [10] D.E. MacLaughlin, J.D. Williamson and J. Butterworth, *Phys. Rev. B* **4**, 60 (1971).